Journal of Associated Medical Sciences 2021; 54 (3): 48-56

JAMS
Journal of Associated Medical Sciences

Thai-Journal Citation Index Centre (TCI) & ASEAN Citation Index (ACI)

Journal of Associated Medical Sciences

Journal homepage: https://www.tci-thaijo.org/index.php/bulletinAMS/index

Measurement of the distribution of neutrons produced by a 15 MV linear accelerator in a solid water phantom using CR-39 detectors

Kasama Homkhaow[1] Thiansin Liamsuwan[1*] Sawanee Suntiwong[2] Natch Rattanarungruangchai[3] Waraporn Sudchai[3]

[1]Faculty of Medicine and Public Health, HRH Princess Chulabhorn College of Medical Science, Chulabhorn Royal Academy, Bangkok, Thailand
[2]Radiation Oncology Department, Chulabhorn Hospital, Chulabhorn Royal Academy, Bangkok, Thailand
[3]Nuclear Technology Service Center, Thailand Institute of Nuclear Technology (Public Organization), Nakorn Nayok Province, Thailand

ARTICLE INFO

Article history:
Received April 2021
Received in revised form April 2021
Accepted as revised June 2021
Available online June 2021

Keywords:
CR-39 detector, neutron dosimetry, nuclear track density, high energy photon therapy

ABSTRACT

Background: In high energy photon therapy with >10 MV x-rays, neutrons are produced from photonuclear reactions between high energy photons and high atomic number materials in the treatment head. Although neutron dose is expected to be relatively small compared to the primary photon dose to the target, neutrons have high quality factors that are associated with the increased secondary cancer risk of the treated patient. Due to the attenuation of neutrons by the patient's body, the distribution of neutron doses at different positions in the patient should be determined for the assessment of organ-specific secondary cancer risks.

Objectives: To determine the distribution of neutrons from a 15 MV linear accelerator at different lateral distances from the isocenter and at different depths in a solid water phantom, as a mimic for the patient body.

Materials and methods: The distribution of neutrons was measured with BARYOTRAK CR-39 detectors in term of nuclear track densities in the CR-39 detectors. A half of the detector's surface area was covered with a boron converter and a polyethylene radiator for thermal and fast neutron measurement, while the other half had no boron converter making it only sensitive to fast neutrons. The detectors were placed in a solid water phantom at 0, 5, 10 and 15 cm lateral distances from the isocenter and at 0, 3, 7, 11, 15 and 18 cm depths from the phantom surface. The detectors were irradiated with 15 MV photon beams at 0° gantry angle for the field size of 20x20 cm^2.

Results: The nuclear track density initially increased with depth, reached a maximum at 3 cm depth and decreased with depth beyond the depth of the maximum. The contributions from fast and thermal neutrons at shallow depths were competitive while at large depths most of neutrons became thermalized. The lateral distribution of the track density had a maximum at the central axis. Thermal neutrons were responsible for this behavior. In contrast, nuclear track densities generated by fast neutrons were nearly constant with the off-axis distance.

Conclusion: Nuclear track densities generated by neutrons varied with the depth and the lateral distance from the isocenter. The conversion coefficients from nuclear track density to dose should consider the energy spectrum of neutrons especially at shallow depths.

* **Corresponding author.**
Author's Address: *Faculty of Medicine and Public Health, HRH Princess Chulabhorn College of Medical Science, Chulabhorn Royal Academy, Bangkok, Thailand.*
** **E-mail address:** thiansin.lia@pccms.ac.th
doi:
E-ISSN: 2539-6056

Introduction

In radiotherapy with high energy photons of >10 MV nominal energy, neutrons are produced from photonuclear reactions between high energy photons and high atomic number materials in the treatment head including primary collimator, target, flattening filter, jaws and shielding materials.[1, 2] Neutron production in the treatment head results in unnecessary radiation exposure to the patient. Although neutron dose is expected to be relatively small compared to the primary dose to the target, neutrons have high quality factors[3] and the exposure of neutrons increases the risk of developing secondary malignancies in the patient.[4] Therefore, neutrons produced by medical linear accelerators operated at energies larger than 10 MV should not be neglected in the radiation protection consideration for radiotherapy patients. Moreover, to determine organ-specific secondary cancer risks, the distribution of neutron doses at different positions in the patient is required.[5]

Previous measurements of photoneutrons from linear accelerators were mostly done in air,[6, 7] on the surface of the patient[8] or on the treatment couch.[9, 10] However, using in-air or surface neutron dose for estimating neutron dose in an organ leads to incorrect dose values because the average neutron energy in air or at the surface could be about 71.4%. different from that found *in vivo*.[11, 12]

In vivo measurements of neutrons are difficult to perform as they are invasive. Therefore, determination of neutron doses in patients receiving radiation therapy are limited to Monte Carlo simulations and in-phantom measurements. In general, the Monte Carlo simulation is considered to be accurate but needs realistic machine modelling and relatively long computational time to produce reasonable results.[13] The machine geometry is sometimes too complex to be modelled with simple mathematical expressions. In that case, the uncertainty related to machine modelling and geometry accuracy effect is not avoidable.[13] Moreover, for events that have relatively low probabilities, for example, neutron generation in photon treatment rooms, a large number of initial particles or radiations need to be simulated to produce dose with acceptable statistical uncertainties. In contrast, in-phantom measurement is easier to perform and mimics the measurement in a patient.

Several groups have performed in-phantom neutron dose measurements. For example, Awotwi-Pratt and Spyrou[14] reported measured neutron dose equivalent as a function of depth and distance from the field edge for 5x5 cm^2, 10x10 cm^2 and 20x20 cm^2 field sizes from a Varian Clinac 2100C linear accelerator operated at 15 MV using bubble detectors. For all field sizes, the neutron dose equivalent was found to maximize at 1 cm depth in a water phantom and at 0 cm distance from field edge, in agreement with d'Errico *et al*.'s experiment performed with an 18 MV linear accelerator at 10x10 cm^2 field size.[15] Yücel *et al*.[16] measured neutron fluxes from an 18 MV Varian Clinac DHX dual energy linear accelerator at 0, 5 and 10 cm depths in a solid water phantom for the field size of 20x20 cm^2 using the foil activation method. The neutron flux was found to maximize at 5 cm depth, providing the maximum neutron dose of about 0.64±0.04 mSv per Gy of photon prescribed dose. Dawn *et al*.[17] measured in-field photoneutron fluences at difference depths in a tissue equivalent phantom irradiated by 15 MV photons from TrueBeam and Novalis Tx linear accelerators for the field size of 30x30 cm^2 using polyallyl diglycol carbonate (PADC) or CR-39 detectors. The fast neutron fluence from both accelerator models had a maximum at the phantom surface and decreased with the depth in the phantom, while the thermal neutron dose peaked at 3 and 6 cm depths for TrueBeam and Novalis Tx, respectively.

Since each neutron detector has different responses to different neutron energy spectra, detector selection should be done appropriately.[18] CR-39 detectors are particularly useful for neutron dose determination in high energy x-ray therapy because they are insensitive to photons, require no electronic equipment, have non-fading signals and are tissue equivalent.[19] When neutrons collide with the polymeric structure of the CR-39 detector, proton and carbon recoils are generated from elastic scattering, inducing latent damage regions.[18] In addition, CR-39 detectors can be modified to detect thermal neutrons by using a converter made of boron (^{10}B) or lithium (^{6}Li) placed on top of the detectors.[20, 21] Neutron dose is converted from nuclear track density obtained by CR-39 measurement using an appropriate calibration coefficient. Since CR-39 detectors have been used for personal dose monitoring for many years[22-24], the calibration of these detectors are usually based on standard neutron sources such as $^{241}Am/Be$ and ^{252}Cf.[25] However, it is not clear whether a calibration coefficient obtained from a standard source is also valid for neutron measurement in a radiation field generated by high energy linear accelerator such as the Varian TrueBeam linear accelerator (Varian Medical System, Palo Alto, CA, USA). This is because a standard source produces a different neutron spectrum than that produced in the treatment room. Thus, converting the nuclear track density generated in the detector to dose by using the calibration coefficient obtained from a measurement with a standard source may provide incorrect neutron dose.

The objective of this work was to determine the distribution of neutrons, in term of nuclear track densities in CR-39 detectors, in a solid water phantom mimicking a patient receiving 15 MV X-rays from the TrueBeam linear accelerator (Varian Medical System, Palo Alto, CA, USA), to be used for determination of location-specific calibration coefficients in conjunction with Monte Carlo simulation (more detail in Discussion). The detectors were placed at different distances from the isocenter and at different depths in the solid water phantom. The relationship between the nuclear track density and the measurement position as well as the distribution of fast and thermal neutrons are presented in this paper.

Materials and methods

CR-39 detectors

The CR-39 detectors used in this study were BARYOTRAK neutron detectors (Nagase Landauer, Ltd., Japan). BARYOTRAK consists of a CR-39 plastic sheet with the dimension of 15.50 mm x 9.34 mm x 0.86 mm. The CR-39 sheet was put into a plastic holder with a half of the surface area covered with a boron converter (Teflon® doped with boron-10) and a polyethylene radiator and the other half with only a polyethylene radiator, as shown in Figure 1. Fast neutrons are detected in both areas covered by the polyethylene radiator through neutron-proton elastic scattering that converts fast neutrons to recoil protons. Since thermal neutrons have relatively low probability of elastic scattering but relatively high probability of neutron capture reaction, the boron converter is used to induce $^{10}B(n,\alpha)^{7}Li$ reaction for thermal neutron detection. Following these interactions, recoil protons and alpha particles produce latent damages in CR-39 sheets that are associated with fast neutrons and thermal neutrons, respectively. Figure 2 shows the conceptual design of the Baryotrak neutron detector.

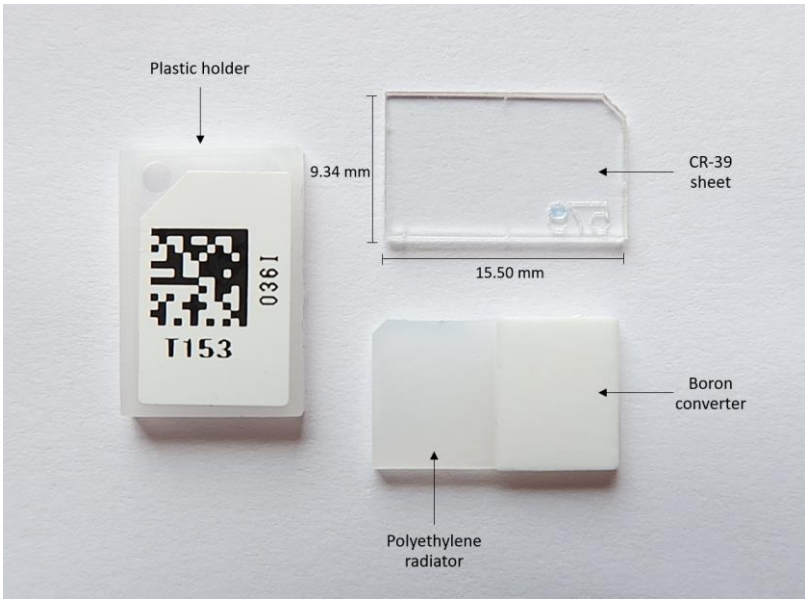

Figure 1. *BARYOTRAK neutron detectors (Nagase Landauer, Ltd., Japan).*

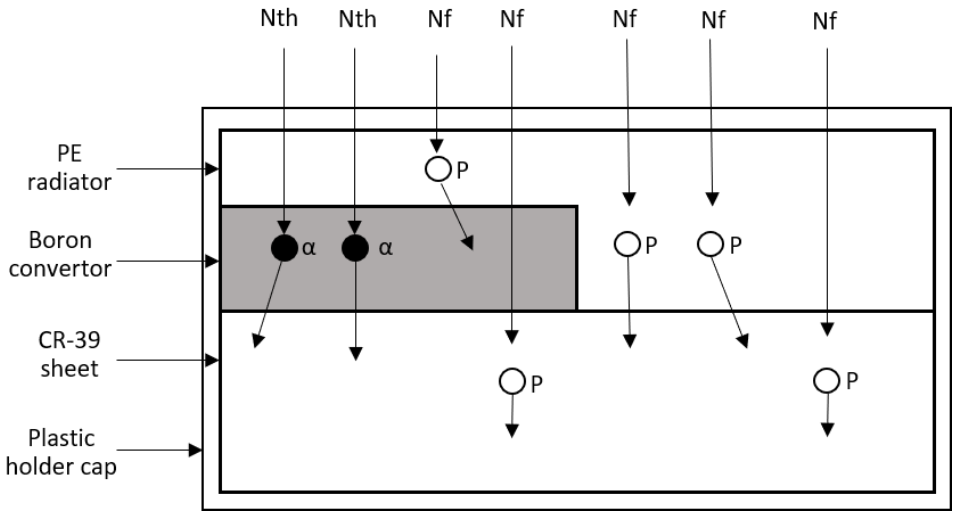

Figure 2. *Neutron detection by BARYOTRAK neutron detectors (side view). Nth: a thermal neutron and Nf: a fast neutron, PE: polyethylene.*

Irradiated CR-39 detectors were etched in a chemical solution of 5.26 M NaOH at a temperature of 72±1 °C for 15 hours and 30 minutes. After the chemical process, tracks produced by the collision of secondary alpha particles or recoil protons on the CR-39 sheets became visible under a microscope. The tracks were discriminated in term of neutron energy (tracks from thermal and fast neutrons) and counted manually using a light microscope (Euromex Microoscopen, Arnhem, Netherland) in an area of 4.5x3 mm^2 of each half of the surface area at a magnification of 400x. The illustration of track counting on the CR-39 detectors can be seen in Figure 3. The number of tracks per square centimeter corresponds to the nuclear track density (tracks/cm^2).

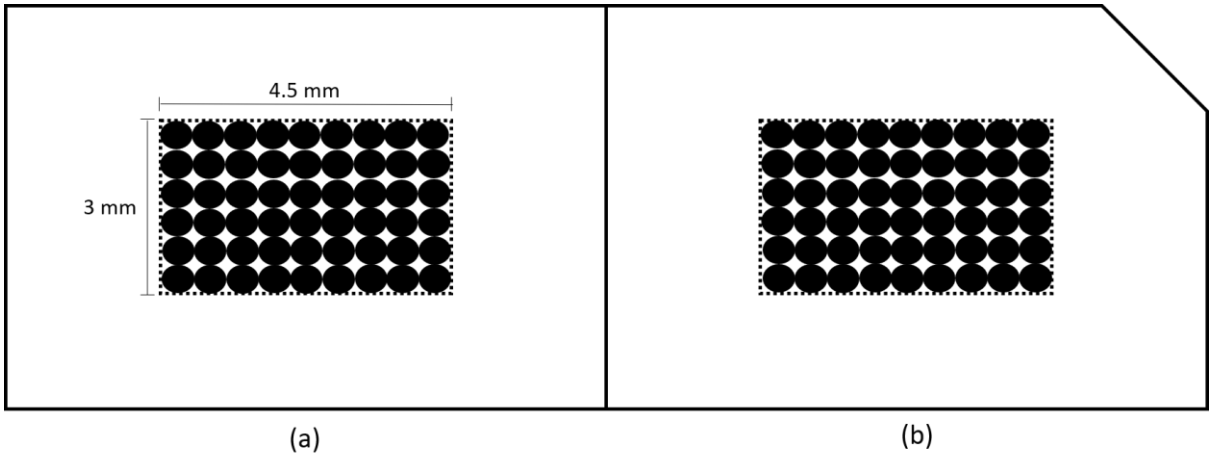

Figure 3. *Illustration of areas used for counting tracks in the CR-39 detectors. The shaded regions are the counting areas, (a): a half of the surface area covered with a boron converter and a polyethylene radiator, (b): the other half of the surface area covered only with a polyethylene radiator.*

Measurement set-up

The CR-39 detectors were placed in a 30x30x22 cm^2 GAMMEX solid water phantom (RMI®, Middleton, WI, U.S.A) at 0, 5, 10 and 15 cm lateral distances from the isocenter in the transverse plane parallel to the treatment couch top and at 0, 3, 7, 11, 15 and 18 cm depths from the phantom surface, as shown in Figure 4. The detectors were sandwiched between boluses, which were used to reduce air gaps between the solid water phantom slabs.

The CR-39 detectors were exposed to the secondary neutron field generated by 15 MV photon beams from the Varian TrueBeam linear accelerator (Varian Medical System, Palo Alto, CA, USA). The irradiation was done at 219.5 MU (2Gy prescribed dose at the isocenter) and the source-to-axis distance (SAD) was 100 cm. The photon beam was delivered to the solid water phantom in one direction (0° gantry angle) with the field size of 20x20 cm^2 at the isocenter. The isocenter was at 11 cm depth from the phantom surface, mimicking the depth representing the average uterine position of patients.[26] The measurement was repeated for 3 times.

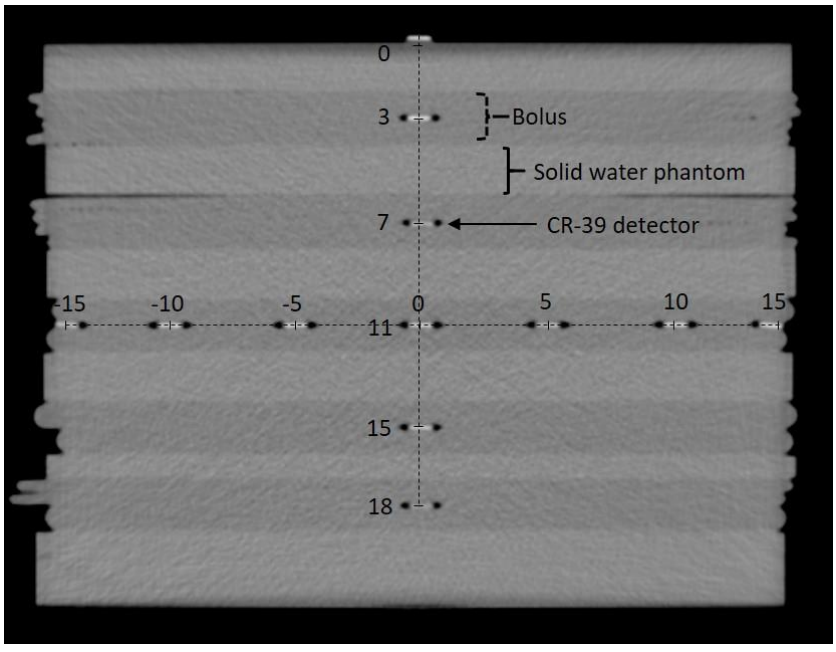

Figure 4. *Placement of CR-39 detectors and boluses (dark grey) in the solid water phantom (light grey) (side view). The scales are in centimeter (cm).*

Results

The microscopic images of tracks in one of the CR-39 detectors after etching are shown in Figure 5. Nuclear tracks generated by thermal neutrons in the detector area covered with the boron converter were larger in size than those produced by fast neutron tracks because thermal neutrons were converted to alpha particles that are heavier than recoil protons converted from fast neutrons. In most cases, tracks were nearly spherically symmetric. However, when a neutron hit the CR-39 detector in the direction that was not perpendicular to the CR-39 detector, a tail of the track could be seen in the microscopic image, as shown in Figure 5c.

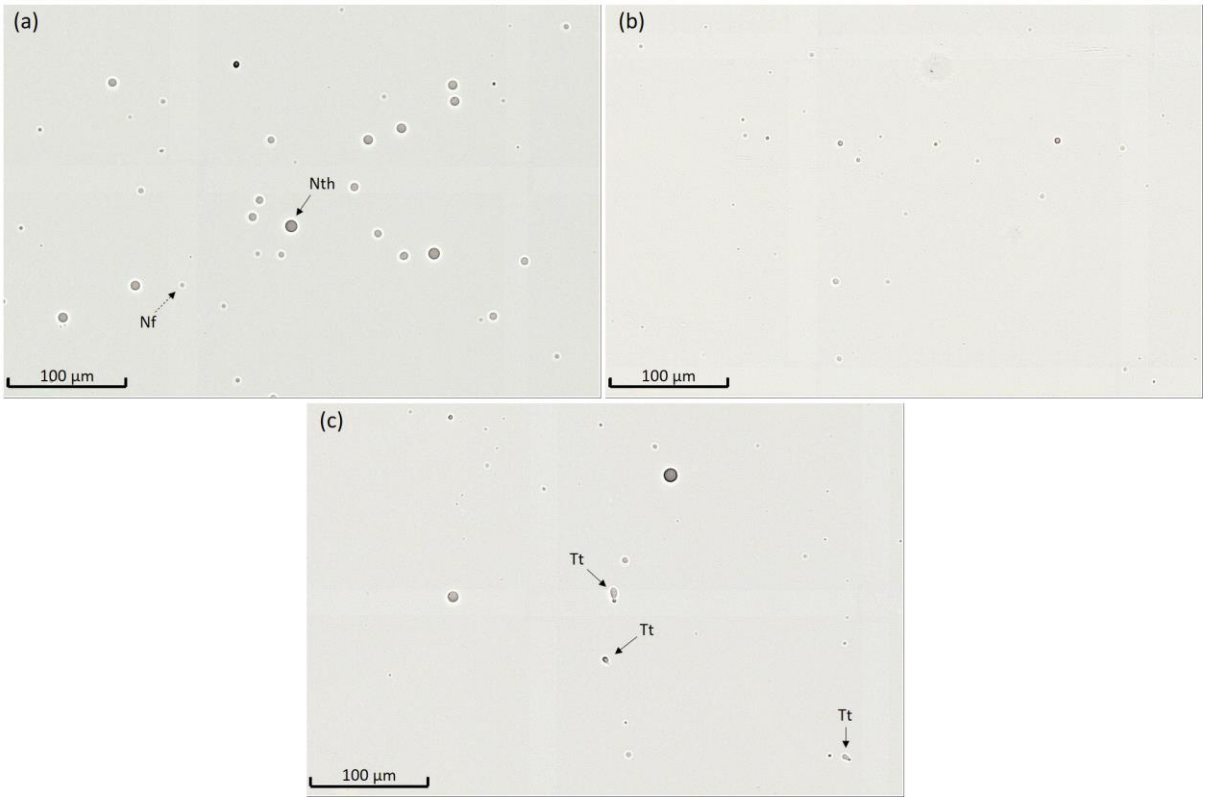

Figure 5*. Microscopic images of tracks obtained from CR-39 measurement. (a): detector area covered with boron converter, (b): other area without boron converter, (c): tracks produced when neutrons hit the CR-39 detector in the directions that were not perpendicular to CR-39 detector, Nth: tracks from thermal neutrons, Nf: tracks from fast neutrons, Tt: track from a neutron hitting the CR-39 detector in the direction that was not perpendicular to CR-39 detector.*

Figure 6 shows the nuclear track density as a function of depth in the solid water. For each measurement, the nuclear track density increased with depth until it reached a maximum at 3 cm depth in the solid water phantom. Beyond the depth of the maximum, track density decreased with depth and was similar to the percentage depth dose of photons. Figure 6 also shows the nuclear track densities induced by thermal neutrons and fast neutrons as functions of depth in solid water phantom. Nuclear track densities induced by fast neutrons maximized at the surface and decreased with the depth in solid water phantom. In contrast, the track densities induced by thermal neutrons, first, increased with the depth until it reached a maximum at a 3 cm depth in solid water phantom. Beyond the depth of the maximum, track densities from thermal neutrons decreased with the depth

Figure 7 shows the lateral distribution of track densities at different distances from the isocenter (at 11 cm depth). The maximum values of track densities were at the center of the radiation field (0 cm distance from isocenter), and the track density decreased when the distance from the isocenter was increased. Moreover, it was found that the track density induced by thermal neutrons maximized at the central axis of the photon beam and rapidly decreased when the distance from the isocenter was increased. In contrast, the track densities from fast neutrons were relatively constant with the distance away from the isocenter.

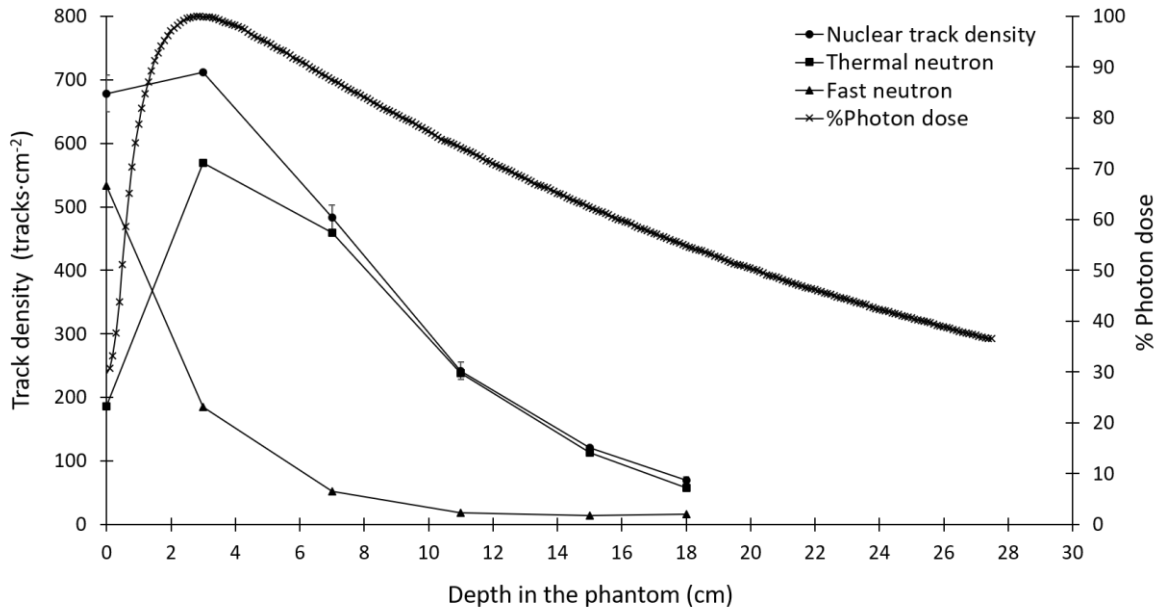

Figure 6. *Nuclear track density as a function of depth in solid water phantom (left ordinate) compared to the photon depth dose distribution (right ordinate).*

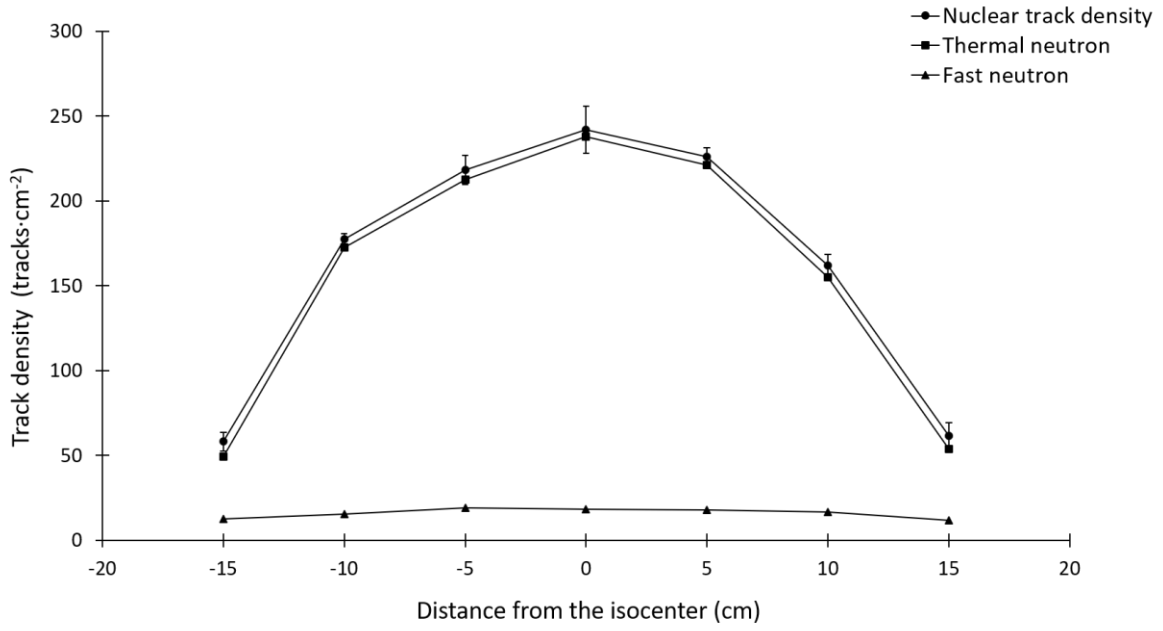

Figure 7. *Lateral distribution of track densities at the isocenter depth (11 cm depth).*

Discussion

In this work, nuclear track densities in CR-39 neutron detectors were measured in a solid water phantom irradiated with 15 MV photon beams from the TrueBeam linear accelerator for the field size of 20x20 cm^2. The nuclear track density is proportional to the number of neutrons hitting the detector per unit area.

From the measurement, it was found that the track density initially increased with depth, reached a maximum at 3 cm depth and decreased with depth beyond the depth of the maximum, in agreement with previous reports.[12, 27, 28] The buildup of the track density arose from the competitive processes between the moderation of fast neutrons from the accelerator head by elastic scattering with hydrogen atoms and the absorption of thermal neutrons.

The nuclear track density as a function of lateral distance from the isocenter showed a maximum at the central axis. The track density induced by thermal neutrons maximized at the central axis and decreased with the distance away from the isocenter while the track density induced by fast neutrons was relatively constant with the off-axis distance. The maximum track density at the central axis indicated that the forward-directed neutrons originated by the highest energy photons were likely to be produced along the central beam axis. Similar observations have been reported by Awotwi-Pratt and Spyrou[14] and Brkić *et al*.[29]

Evaluation of neutron dose from the CR-39 measurement, the track density needs to be converted to neutron dose by using an appropriate conversion coefficient obtained from the measurement in a neutron standard field similar to that present during the detector usage due to the energy dependence of the neutron detectors.[11] The detectors used in this study have been calibrated for personal dose monitoring purposes in term of $H_p(10)$ in standard neutron fields of a bare ^{252}Cf source, a D_2O moderated ^{252}Cf source, an $^{241}Am/Be$ source and a graphite pile moderated ^{252}Cf source (thermal neutrons). However, it is not clear whether $H_p(10)$ measured in the standard sources is valid for neutron measurement in a radiation field generated by the high energy linear accelerator. This is because a standard source produces a different neutron spectrum than that produced in the treatment room. Since standard neutron fields similar to those present in the phantom are not available,[25] neutron dose obtained from a Monte Carlo simulation can be used as the reference dose to evaluate position-specific neutron track density-to-dose conversion coefficients of the CR-39 detector. In the future work, we will perform a Monte Carlo simulation to evaluate the neutron spectra at different positions in the solid water phantom to determine the nuclear track density-to-dose conversion coefficients at different depths and off-axis distances in the phantom.

Conclusion

In the present study, CR-39 detectors were used to measure the distribution of neutrons inside a solid water phantom at different depths and at different lateral distances from the isocenter. The results are presented in term of nuclear track densities, which are related to neutron fluence and neutron doses. It was found that the nuclear track density initially increased with depth and reached a maximum at 3 cm depth in the solid water phantom, beyond the depth of the maximum the nuclear track density decreased with depth. The lateral distribution of nuclear track densities in the isocenter plane (at 11 cm depth) showed a maximum at the central axis and decreased with the off-axis distance. Thermal neutrons were responsible for this behavior. In contrast, nuclear track densities induced by fast neutrons were relatively constant with the off-axis distance. The current study indicated that the contribution of fast and thermal neutrons to total neutron dose varied with the depth in the phantom but only the contribution of thermal neutrons varied with the off-axis distance from the isocenter. The conversion coefficients from nuclear track density to dose should consider the different neutron spectra inside the phantom for the accurate evaluation of neutron doses. The result of this work can be used together with the Monte Carlo simulation to estimate position-specific neutron track density-to-dose conversion coefficients of the CR-39 detector. Such conversion coefficients can be directly used with the CR-39 detector to determine neutron dose in patients or in phantoms with a higher accuracy compared to using conversion coefficients typically obtained from standard measurements.

Conflict of interest

The authors declare that there is no conflict of interest.

References

[1] Kry SF, Bednarz B, Howell RM, Dauer L, Followill D, Klein E, et al. AAPM TG 158: measurement and calculation of doses outside the treated volume from external-beam radiation therapy. Med Phys 2017; 44(10): 391-429. doi: 10.1002/mp.12462.

[2] Biltekin F, Yeginer M, Ozyigit G. Investigating in-field and out-of-field neutron contamination in high-energy medical linear accelerators based on the treatment factors of field size, depth, beam modifiers, and beam type. Phys Med 2015; 31(5): 517-23. doi: 10.1016/j.ejmp.2015.03.015.

[3] Nuclear Regulatory Commission and Department of Veterans Affairs. Neutron quality factor. United States: Oak Ridge Inst. for Science and Education; 1995.

[4] Takam R, Bezak E, Marcu L, Yeoh E. Out-of-field neutron and leakage photon exposures and the associated risk of second cancers in high-energy photon radiotherapy: current status. Radiat Res 2011; 176(4): 508-20. doi: 10.1667/rr2606.1.

[5] Schneider U, Zwahlen D, Ross D, Kaser-Hotz B. Estimation of radiation-induced cancer from three-dimensional dose distributions: Concept of organ equivalent dose. Int J of Radiation Oncology* Biol Phys 2005; 61(5): 1510-5. doi: 10.1016/j.ijrobp.2004.12.040.

[6] Chu W, Lan J, Chao T, Lee C, Tung C. Neutron spectrometry and dosimetry around 15 MV linac. Radiat Meas 2011; 46(12): 1741-4. doi: 10.1016/j.radmeas.2011.06.029.

[7] Montgomery L, Evans M, Liang L, Maglieri R, Kildea J. The effect of the flattening filter on photoneutron production at 10 MV in the Varian TrueBeam linear accelerator. Med Phys 2018; 45(10): 4711-9. doi: 10.1002/mp.13148.

[8] Reft CS, Runkel-Muller R, Myrianthopoulos L. In vivo and phantom measurements of the secondary photon and neutron doses for prostate patients undergoing 18 MV IMRT. Med Phys 2006; 33(10): 3734-42. doi: 10.1118/1.2349699.

[9] Alem-Bezoubiri A, Bezoubiri F, Badreddine A, Mazrou H, Lounis-Mokrani Z. Monte Carlo estimation of photoneutrons spectra and dose equivalent around an 18 MV medical linear accelerator. Radiat Phys Chem 2014; 97: 381-92. doi: 10.1016/j.radphyschem.2013.07.013.

[10] Ipe NE, Roesler S, Jiang S, Ma C, editors. Neutron measurements for intensity Modulated Radiation therapy. Proceedings of the 22nd Annual International Conference of the IEEE Engineering in Medicine and Biology Society (Cat No 00CH37143); 2000: IEEE.

[11] Hälg RA, Besserer J, Boschung M, Mayer S, Clasie B, Kry SF, et al. Field calibration of PADC track etch detectors for local neutron dosimetry in man using different radiation qualities. Nucl Instrum Methods Phys Res, A 2012; 694: 205-10. doi: 10.1016/j.nima.2012.08.021.

[12] Kry SF, Howell RM, Salehpour M, Followill DS. Neutron spectra and dose equivalents calculated in tissue for high-energy radiation therapy. Med Phys 2009; 36(4): 1244-50. doi: 10.1118/1.3089810.

[13] Seco J, Verhaegen F., editors. Monte Carlo techniques in radiation therapy. Florida: CRC press; 2013.

[14] Awotwi-Pratt J, Spyrou N. Measurement of photoneutrons in the output of 15 MV varian clinac 2100C LINAC using bubble detectors. J Radioanal Nucl Chem 2007; 271(3): 679-84. doi: 10.1007/s10967-007-0325-8.

[15] d'Errico F, Nath R, Tana L, Curzio G, Alberts WG. In-phantom dosimetry and spectrometry of photoneutrons from an 18 MV linear accelerator. Med Phys 1998; 25(9): 1717-24. doi: 10.1118/1.598352.

[16] Yücel H, Çobanbaş İ, Kolbaşı A, Yüksel AÖ, Kaya V. Measurement of photo-neutron dose from an 18-MV medical linac using a foil activation method in view of radiation protection of patients. Nucl Eng Technol 2016; 48(2): 525-32. doi: 10.1016/j.net.2015.11.003.

[17] Dawn S, Pal R, Bakshi A, Kinhikar R, Joshi K, Jamema S, et al. Evaluation of in-field neutron production for medical LINACs with and without flattening filter for various beam parameters-Experiment and Monte Carlo simulation. Radiat Meas 2018; 118: 98-107. doi: 10.1016/j.radmeas.2018.04.005.

[18] Farhood B, Ghorbani M, Goushbolagh NA, Najafi M, Geraily G. Different methods of measuring neutron dose/fluence generated during radiation therapy with megavoltage beams. Health Phys 2020; 118(1): 65-74. doi: 10.1097/HP.0000000000001130.

[19] Kumar V, Sonkawade R, Dhaliwal A. Optimization of CR-39 as neutron dosimeter. Indian J Pure Appl Phys 2010; 48(7): 466-9.

[20] Oda K, Miyake H, Michijima M. CR39-BN detector for thermal neutron dosimetry. Nucl Sci Tech 1987; 24(2): 129-34. doi: 0.3327/jnst.24.129

[21] Mameli A, Greco F, Fidanzio A, Fusco V, Cilla S, D'Onofrio G, et al. CR-39 detector based thermal neutron flux measurements, in the photo neutron project. Nucl Instrum Methods Phys Res Section B: Beam Interactions with Materials and Atoms 2008; 266(16): 3656-60. doi: 10.1016/j.nimb.2008.05.122.

[22] García M, Amgarou K, Domingo C, Fernández F. Neutron response study of two CR-39 personal dosemeters with air and Nylon converters. Radiat Meas 2005; 40(2-6): 607-11. doi: 10.1016/j.radmeas.2005.04.017.

[23] Pal R, Nadkarni VS, Naik D, Beck M, Bakshi AK, Chougaonkar MP, et al. Development and dosimetric characterization of indigenous PADC for personnel neutron dosimetry. Nucl Technol Radiat Prot 2015; 30(3): 175-87. doi: 10.2298/NTRP1503175P.

[24] Romero-Expósito M, Martínez-Rovira I, Domingo C, Bedogni R, Pietropaolo A, Pola A, et al. Calibration of a Poly Allyl Diglycol Carbonate (PADC) based track-etched dosimeter in thermal neutron fields. Radiat Meas 2018; 119: 204-8. doi: 10.1016/j.radmeas.2018.11.007.

[25] Thomas D, Bedogni R, Méndez R, Thompson A, Zimbal A. Revision of ISO 8529—reference neutron radiations. Radiat Prot Dosim 2018; 180(1-4): 21-4. doi: 10.1093/rpd/ncx176.

[26] Oonsiri P, Vannavijit C, Wimolnoch M, Suriyapee S, Saksornchai K. Estimated radiation doses to ovarian and uterine organs in breast cancer irradiation using radio-photoluminescent glass dosimeters (RPLDs). J Med Radiat Sci 2020; 68: 167-174. doi: 10.1002/jmrs.445.

[27] Rezaian A, Nedaie HA, Banaee N. Measurement of neutron dose in the compensator IMRT treatment. Appl Radiat Isot 2017; 128: 136-41. doi: 10.1016/j.apradiso.2017.06.013.

[28] Martinez-Ovalle S, Barquero R, Gomez-Ros J, Lallena A. Neutron dose equivalent and neutron spectra in tissue for clinical linacs operating at 15, 18 and 20 MV. Radiat Prot Dosim 2011; 147(4): 498-511. doi: 10.1093/rpd/ncq501.

[29] Brkić H, Ivković A, Kasabašić M, Sovilj MP, Jurković S, Štimac D, et al. The influence of field size and off-axis distance on photoneutron spectra of the 18 MV Siemens Oncor linear accelerator beam. Radiat Meas 2016; 93: 28-34. doi: 10.1016/j.radmeas.2016.07.002